Cr 2 AlC high temperature oxidation under dry and wet air: understanding of the oxidation mechanism

A. Zuber, V. Gauthier-Brunet, J. Roger, J. Gonzalez-Julian, T. Ouisse, Sylvain Dubois

Cr_2AlC high temperature oxidation under dry and wet air: understanding of the oxidation mechanism

A. Zuber[1*], V. Gauthier-Brunet[1], J. Roger[2], J. Gonzalez-Julian[3], T. Ouisse[4] and S. Dubois[1]

[1] Institut PPRIME, CNRS/Université de Poitiers/ENSMA, UPR 3346, TSA 41126, 86073, Poitiers Cedex 9, France.

[2] Université de Bordeaux, CNRS, Laboratoire des Composites Thermo-Structuraux, UMR 5801, 33600, Pessac, France.

[3] Chair of Ceramics, Institute of Mineral Engineering (GHI), RWTH Aachen University, Forckenbeckstrasse 33, 52074 Aachen, Germany

[4] Université Grenoble-Alpes, CNRS, Grenoble INP, LMGP, 38000 Grenoble, France

*corresponding author email address: axel.zuber@univ-poitiers.fr

Abstract

Cr_2AlC is one of the most interesting MAX phase compositions to operate under aggressive environments up to 1400 °C, but the effect of humidity at high temperatures is still poorly investigated. Cr_2AlC high-temperature oxidation tests under controlled humidity are carried out on fined-grained samples for 40 hours in the [1000-1400 °C] temperature range and compared to a previous study performed on single-crystals, fine and coarse-grained samples oxidized under dry air. Oxidation products are characterized and mass gain curves are analysed using both cubic and paralinear oxidation models to extract kinetics and characterize gas emission during the oxidation tests. These experimental data are supported by thermodynamic calculations in order to propose a quite complete oxidation mechanism for Cr_2AlC.

The nature and the arrangement of the oxidation products formed during wet and dry air oxidation tests are similar - a continuous Al_2O_3 layer and a Cr_7C_3 sublayer with pores- which demonstrates that the water vapor does not affect significantly the high-temperature oxidation of Cr_2AlC. The acceleration of the oxidation process during wet air tests is correlated to the higher partial pressure of gaseous species produced in the presence of humidity which is associated with the chromium carbide's volatilization in the form of carbon oxide.

Keywords:

Cr_2AlC, high-temperature oxidation, microstructure, gas emission, thermodynamic calculations

Color should be used for all figures in print.

1. Introduction

Cr_2AlC is one of the most studied and attractive MAX phases (M transition metal, A p-block element and X nitrogen and/or carbon), a well-known class of nanolamellar compounds with an unique combination of metallic and ceramic properties [1]. Cr_2AlC was first discovered in 1963 by Jeitschko et al. [2], but its interest has mainly arisen in the last 10-15 years for its corrosion resistance properties [3]. The structure of Cr_2AlC, first imaged at atomic resolution by Lin et al. [4], is typical of MAX phases: it crystallizes in the $P6_3/mmc$ hexagonal space group and is composed of a stack of M_6X chromium carbide octahedrons layers and aluminium planes. As for other MAX phases such as Ti_2AlC and Ti_3AlC_2, Cr_2AlC is an alumina-forming phase which oxidizes slowly with diffusion based (parabolic, cubic) kinetics and a resulting activation energy typically above 300 $kJ.mol^{-1}$ [3] [5]. These properties make MAX phases comparable to other typical high temperature alloys such as aluminides and superalloys while having higher mechanical properties, as shown in figure 1 [3,6,7].

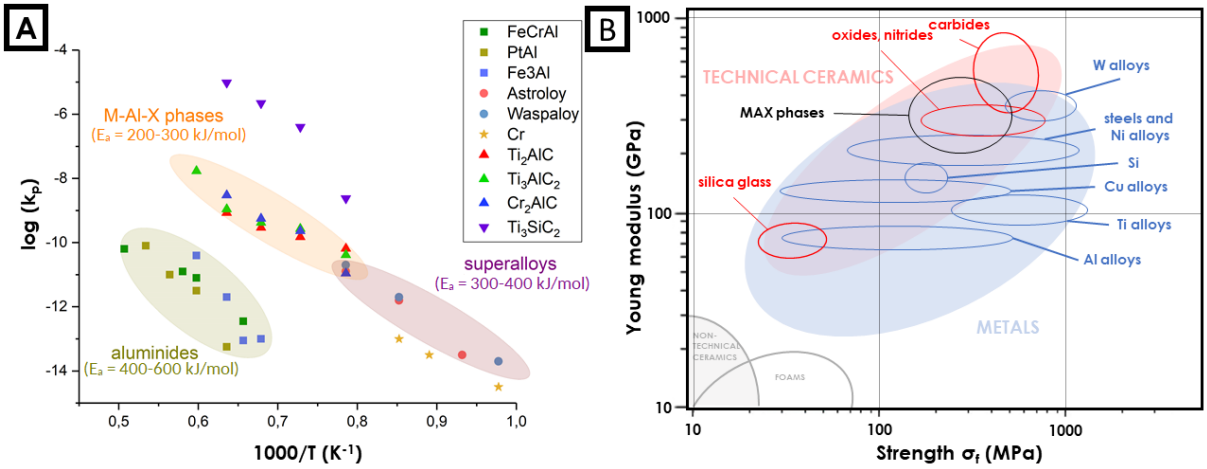

Figure 1: A) Comparison of MAX phases parabolic kinetic constant and activation energy with high-temperature oxidation resistant alloys ones [3-6]. B) Ashby diagram of materials strength vs. Young's modulus reproduced from [7] with MAX phases's position added to it.

Oxidation of bulk Cr_2AlC has been studied in dry and ambient air in a large temperature range, from 700 °C to 1400 °C for various oxidation durations [8-17]. The usual observations made on oxidized Cr_2AlC samples report the formation of an α-Al_2O_3 layer and a Cr_7C_3 chromium carbide sublayer. We recently showed that oxidation in dry air of bulk Cr_2AlC, independently of the grain size, ineluctably involves, for short/mid-term oxidation, the formation of a continuous α-Al_2O_3 layer and a Cr_7C_3 sublayer with pores; whereas very high temperature or long-term oxidation tests lead to the formation of chromia rich corundum's [17]. The pores formation in the carbide sublayer could be caused by Kirkendall effect but it is often explained to be due to carbon and chromium oxides volatilization [8,9,12]. Carbon oxides volatilization was indeed characterized in a unique reference [9] but stays a minor concern in dry air oxidation studies.

Gas volatilization becomes a major concern when performing high-temperature oxidation in wet air due to the water vapor reaction at the oxide surface, which evaporates the oxide scale by forming volatile oxyhydroxides [18,19]. Presence of water vapor can have critical other effects on the global behaviour during the oxidation such as composition and arrangement changes of the oxide scale, oxidation rates increase or oxide scale brittleness [20]. Alumina is usually poorly affected by volatilization in the 1300-1400 °C temperature range, contrary to chromia which undergoes a significant volatilization at temperature as low as 800°C [21]. The influence of water vapor onto the oxidation of MAX phases has been poorly investigated, except in one study of Lin et al. on the wet oxidation of Ti_2AlC and Ti_3AlC_2. The authors mention an oxidation rate increase of these MAX phases in presence of water vapor [21].

In this study, we report the first Cr_2AlC high-temperature oxidation tests under controlled humidity conditions as well as practical and theoretical evidence of carbon oxide volatilization in dry and wet air via paralinear oxidation kinetic model and thermodynamic calculations. For this purpose, fine-grained samples were oxidized in wet air for 40 hours at 1000, 1200 and 1400 °C under three water vapor partial pressures (P_{H_2O}= 1700, 3400, 5100 Pa). For wet oxidation tests, oxidation products were characterized and mass gain curves were treated using both cubic and paralinear models to extract kinetics and oxidation mechanism information for fine-grained samples. Thermodynamic calculations were performed to support the experimental data. Results are compared with a previous study performed on single-crystals, fine and coarse-grained samples oxidized under dry air for 100 hours at temperatures ranging from 800 to 1400 °C [17].

2. Method

2.1. Synthesis method

For the synthesis of fine-grained samples, chromium (Alfa Aesar, purity: 99%, D_{50} = 28.0 µm), aluminium (Alfa Aesar, purity: 99.5%, D_{50} = 9.1 µm) and graphite (Alfa Aesar, purity 99%, D_{50} = 6.9 µm) powders were mixed in a Cr:Al:C=2:1.02:0.97 molar ratio and further with a ball to powder mass ratio of 1:1 during 24h in ethanol using planetary milling. Reactive sintering was performed using a Field Assisted Sintering Technology/Spark Plasma Sintering (FAST/SPS, FCT-HPD5, FCT System GmbH, Germany) under vacuum at 1200°C/30MPa for 15 minutes [17].

For the synthesis of coarse-grained samples, chromium (Alfa Aesar, purity >99%, <44µm), aluminium (Alfa Aesar, purity >99.5%, <44µm) and chromium carbide (Alfa Aesar, purity >99,5%, <44µm) powders were mixed with a Cr:Al:Cr_3C_2=0.525:1.2:0.475 molar ratio and uniaxially cold-pressed. The pellet was then encapsulated into a glass container before being isostatically pressed at 1400 °C/150MPa during 4 hours using a Hot Isostatic Press (ACB-HIP6) [17].

To synthesize the single crystals, aluminium and chromium pellets were melted in an alumina crucible in an induction-heated growth reactor. At 1650°C, a carbon rod was actuated through a hole made in the alumina cover, and dipped at a pre-selected depth into the flux until the dipped part totally dissolved. After carbon dissolution, the flux was cooled down to 1200°C in one week, and then let to cool down freely. Crystals were extracted from the solidified flux by etching in concentrated HCl [17].

2.2. Oxidation processes

For the dry air oxidation tests, the polycrystalline and single crystal samples were cut into parallelepipeds (10x2x2 mm^3) and triangles (half a centimeter square sized plates), respectively. Both were polished with silicon carbide abrasive disks and finished on felt disk with diamond paste of 0.25 µm particles. The polished samples were placed into a thermogravimetric analysis chamber (TGA, SETARAM EVOSYSTEM) and heated under argon flow at 20°C/min. The subsequent isothermal oxidation treatment was performed under dry air flow at T=[800;1500] °C during 100 h. Since previous results related to dry air oxidation tests showed that the oxidation process is independent of the microstructure [17], wet air oxidation tests were carried out only on fine-grained samples. Tests were performed using the same thermogravimetric analysis system, for 40 hours at 1000, 1200 and 1400 °C after heating under dry air. The three water partial pressures used were calculated from the wet gas temperature to be 1700, 3400 and 5100 Pa.

2.3. Kinetic models and data exploitation

Oxidation kinetic constants k_n consist in describing the mass gain Δm over time t, associated to the oxide growth, using a law depending on the reaction mechanism (associated to an order n=1,2,3…) according to $\left(\frac{\Delta m}{S}\right)^n = k_n.t$, with S the sample's surface. For the parabolic and cubic treatments, the normalized mass gain curves were raised to the power 2 and 3 respectively. The slope of the resulting straight line gives the parabolic kinetic constant k_p ($kg^2.m^{-4}.s^{-1}$) and the cubic kinetic constant k_c ($kg^3.m^{-6}.s^{-1}$) at a given temperature.

The paralinear model is used when the mass gain curve is flawed by species volatilization. In the paralinear model, the normalized and smoothed mass gain curve is usually plotted as $\frac{\Delta m}{S}\frac{d\left(\frac{\Delta m}{S}\right)}{dt} f(\frac{-\Delta m}{S}$ [23]. While the parabolic (n=2) and cubic (n=3) models are only diffusion driven growth kinetic models, the paralinear model contains a growth term and a volatilization term expressed as $\frac{\Delta m}{S} = \left(2k_{pl}.t\right)^{1/2} - k_v t$. The intercept of the curve with the y axis is homogeneous to a parabolic kinetic constant and it is further called paralinear kinetic constant k_{pl} ($kg^2.m^{-4}.s^{-1}$). The slope of the curve, called volatilization kinetic constant k_v ($kg.m^{-2}.s^{-1}$), corresponds to a linear kinetic constant. The volatilization kinetic constant k_v can be used to estimate the partial pressure of the volatilized gas P_v according to $P_v \alpha k_v \frac{P_{tot}^{1/2}}{v_{gas}^{1/2}}$, with P_{tot} and v_{gas} the total gas pressure and the gas velocity respectively [19].

For all models, the kinetic constants calculated for each temperature can then be used to obtain the ln(k)=f(1/T) Arrhenius plots and determine the activation energy of the associated oxidation mechanism.

2.4. Thermodynamic calculations

To support the experimental investigations, thermodynamic analyses of Cr_2AlC equilibrium in air were performed with Thermo-Calc software [24]. The thermodynamic equilibria calculated from this software were based on the CALculation of PHAse Diagrams (CALPHAD) methodology [25]. The relevant thermodynamic descriptions of the Cr-Al-C and CrO_2-Al_2O_3 systems reported, respectively by Y. Liang et *al.* and by T. M. Besmann *et al.*, were used for the equilibrium calculations of the system [26,27]. The thermodynamic descriptions of the gaseous species considered for the calculations result from the NIST Chemistry WebBook and the work of B.B. Ebbinghaus [28,29].

2.5. Microstructural characterization

Scanning electron microscopy (SEM - JEOL 7001-TTLS) and energy dispersive X-Ray spectrometry (EDXS, Oxford Instrument) techniques were used to observe the surface and cross-section of the samples and analyse the composition of the different contrasted regions, before and after oxidation. X-Ray Diffraction (XRD - BRUKER D8 diffractometer) with Cu-K_α radiation was performed for crystalline structure identification of synthesized and oxidized samples.

3. Results and discussion

3.1. Microstructure characterization

As reported in [17], Cr_2AlC fine-grained (2 µm) samples contain small amounts of Al_2O_3 and Cr_7C_3 chromium carbide impurities as evidenced on the XRD pattern shown in Figure 2(a).

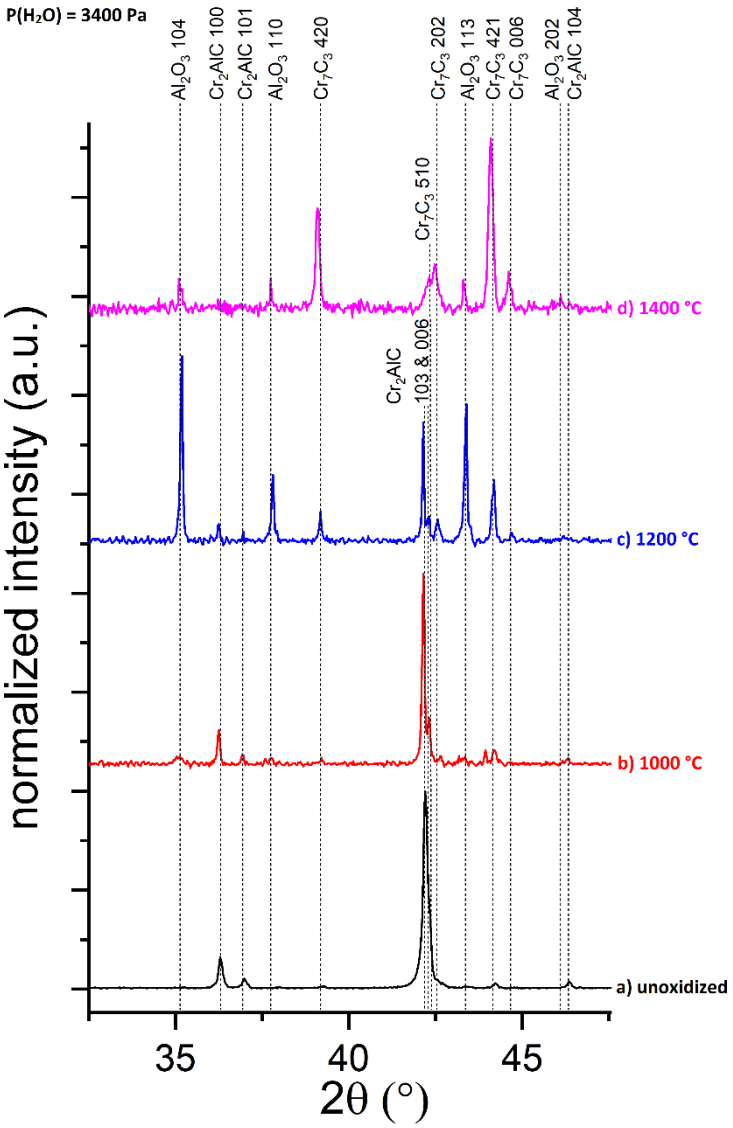

Figure 2: XRD patterns of fine-grained Cr_2AlC samples: (a) before oxidation, and after oxidation at (b) 1000°C, (c) 1200°C, (d) 1400 °C during 40 hours under a water vapor partial pressure of 3400 Pa. The XRD patterns have been indexed with the theoretical structures available on the Materials Project website (Cr_2AlC $P6_3mmc$ mp-9956; Al_2O_3 $R\bar{3}c$ mp-1043; Cr_7C_3 $P6_3mc$ mp-1196316) [30].

After oxidation tests at 1000, 1200 and 1400°C during 40 hours under a water vapor partial pressure of 1700 Pa, the sample's surface consists of a continuous Al_2O_3 layer which undergo buckling and cracking revealing the Cr_7C_3 sublayer (Figure 3). At 1000 °C, θ-Al_2O_3 whiskers have been observed, which is consistent for this oxidation time-temperature conditions. The corresponding cross-section SEM micrographs in back-scattered mode of the oxidized Cr_2AlC fine-grained samples shown in Figure 4 confirm the presence of an external alumina layer and a chromium carbide sublayer, as reported in the case of dry air oxidation tests [17]. The only difference is related to the existence of numerous and large porous areas in the Cr_7C_3 sublayer and to an increase of the alumina scale thickness after wet oxidation tests implying an acceleration of the oxidation process. For brevity, the SEM micrographs related to samples oxidized at others water vapor partial pressures are not shown here since they exhibit similar features. Nevertheless, table 1 shows variation of the alumina thickness measured on the different micrographs. The alumina scale's thickness of the samples oxidized in dry air during 100 hours is the same as the one measured on samples oxidized in wet air for 40 hours, suggesting an acceleration of the oxidation process in the presence of water vapor.

However, the scale's thickness shows no obvious dependency on the water vapor partial pressure, suggesting that the water is an accelerating factor but doesn't significantly contribute to the oxidation process.

From the XRD patterns reported in Figure 2, the intensity of the peaks associated to Cr_7C_3 and Al_2O_3 phases increases with the oxidation temperature while the peaks associated to the Cr_2AlC fades, indicating a substantial increase of the chromium carbide and alumina layers thickness with the oxidation temperature in good agreement with Table 1. These observations, related to a water vapor partial pressure of 3400 Pa, are also valid for other partial pressures.

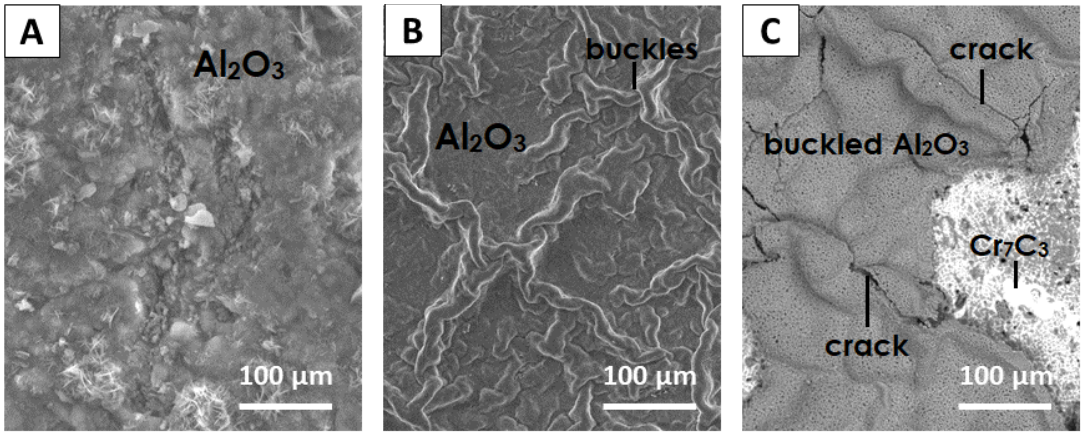

Figure 3: SEM micrographs of fine-grained Cr_2AlC sample's surface oxidized at: A) 1000 °C, B) 1200 °C, and C) 1400 °C during 40 hours under wet air (P_{H_2O} = 1700 Pa).

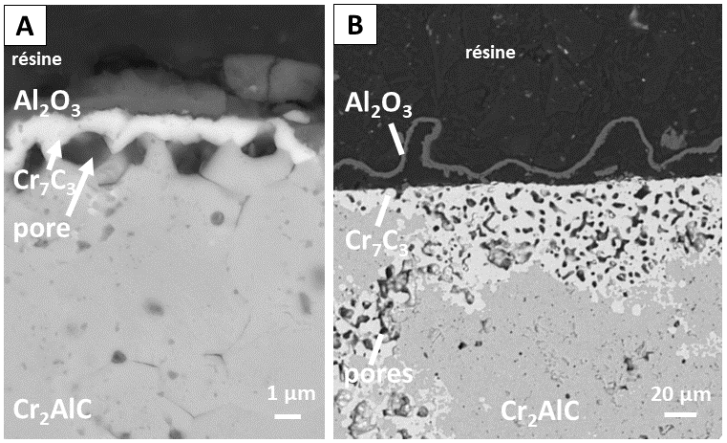

Figure 4: Cross-section SEM micrographs, in back-scattered mode, of a fine-grained Cr_2AlC sample oxidized at: A) 1000°C and B) 1200 °C during 40 hours under wet air (P_{H_2O} = 1700 Pa)

	Al_2O_3 scale thickness on fine grained samples (µm)		
	0 Pa, 100 h	1700 Pa, 40 h	3400 Pa, 40 h
1000 °C	1 ±0.5	1 ±0.5	2 ±0.5
1200 °C	5 ±1	4 ±1	5 ±1
1400 °C	17±2	14 ±1	14 ±1

Table 1. Thickness of the alumina scale for several temperature and water vapor partial pressure conditions measured on Cr_2AlC fine-grained samples after 40 h and 100 h oxidation. The uncertainties are representative of the local variation of the alumina scale thickness measured on cross-sectional SEM micrographs.

This first part shows that one of the features making Cr_2AlC remarkable is its similar oxidation behaviour in the 800-1400°C temperature range in dry air and wet air. Indeed, the oxide layer formed during the wet and dry oxidation tests consists in a continuous external Al_2O_3 layer and a Cr_7C_3 porous sublayer in contact with the fine-grained Cr_2AlC phase. Regarding the nature and the arrangement of the oxidation products, one can conclude that the water vapor does not affect the high-temperature oxidation of Cr_2AlC in a significant way, at least for the investigated partial pressures and oxidation times. This statement has however to be confronted to other studies in similar conditions which are scarce in the literature.

3.2. Kinetics coupled with thermodynamic calculations

3.2.1.Mass gain curves

The mass gain curves are measured as a function of time during the wet air oxidation process for the three temperatures and water vapor partial pressures investigated (Figure 5). Compared to the dry conditions tests, the global behaviour under wet conditions shows a similar increase of the mass gain with temperature but does not reveal any clear tendency with the water vapor partial pressure. One can observe that the dry air oxidation curve's slope tilts more rapidly at 1400 °C than the one of the samples oxidized under wet air, highlighting the change of mechanism in the case of dry air oxidation tests compared to wet air tests.

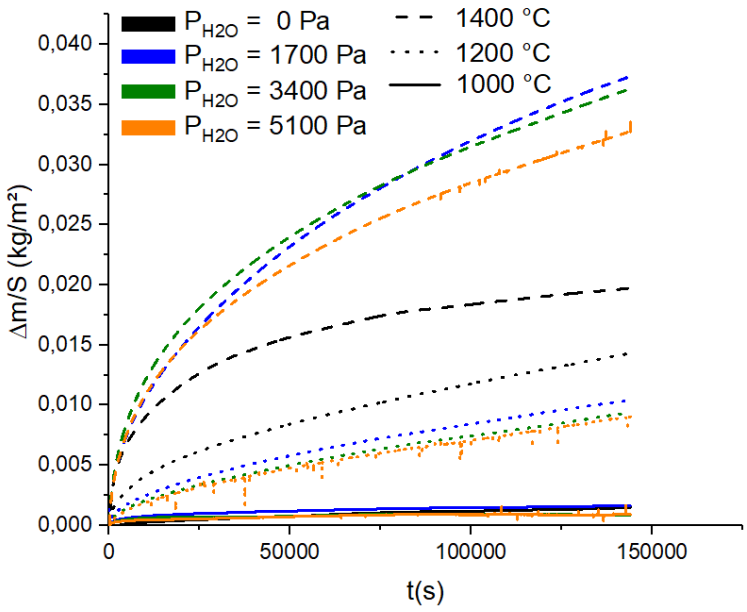

Figure 5: Normalized mass gain curves of fine-grained Cr_2AlC samples oxidized during 40 hours at T=[1000; 1200; 1400] °C and at P_{H_2O} =[1700; 3400; 5100] Pa. N.B.: In our previous article [16], the mass gain curves were not normalized (/100) ; these curves are the normalized ones.

The exploitation of the mass gain curves for the Cr_2AlC single-crystal, coarse-grained and fine-grained polycrystalline samples [17] using the cubic, parabolic and paralinear models gives the kinetic constants listed in Table 2, for dry air and wet air oxidation tests. Independently of the microstructure, the k_p parabolic and k_{pl} paralinear kinetic constant values are close to each other, demonstrating that the oxide scale growth is well-described without considering species volatilization. Despite that, trying to take a volatilization phenomenon into account reveals differences between dry and wet air oxidation, as well as differences between oxidation tests performed below and above 1200 °C. The volatilization kinetic constant values, in the case of oxidation tests performed under dry air and below 1200°C, are quite low, in the range 5×10^{-9} - 5×10^{-8} mg/mm²/s. In the case of oxidation tests performed under dry air above 1200 °C and under wet air, the volatilization kinetic constant values are higher, in the range 8×10^{-8} - 7×10^{-7} mg/mm²/s. These features are valid whatever the microstructure of the Cr_2AlC sample.

T (°C)	P(H_2O) (Pa)	k_c ($kg^3.m^{-6}.s^{-1}$)	k_p ($kg^2.m^{-4}.s^{-1}$)	k_{pl} ($kg^2.m^{-4}.s^{-1}$)	k_v ($kg.m^{-2}.s^{-1}$)
800 (SC)	0	4.7×10^{-12}	80×10^{-11}	8.7×10^{-11}	2.3×10^{-8}
900 (SC)	0	3.0×10^{-13}	6.1×10^{-11}	1.2×10^{-10}	1.7×10^{-8}
1000 (SC)	0	3.3×10^{-13}	6.0×10^{-11}	2.4×10^{-11}	5.3×10^{-9}
1100 (SC)	0	1.1×10^{-11}	6.4×10^{-10}	8.9×10^{-10}	4.6×10^{-8}
1200 (SC)	0	1.4×10^{-9}	1.7×10^{-8}	9.0×10^{-9}	4.4×10^{-8}
1300 (SC)	0	4.3×10^{-10}	7.7×10^{-9}	7.2×10^{-9}	8.5×10^{-8}
1400 (SC)	0	1.7×10^{-7}	4.3×10^{-7}	2.5×10^{-7}	1.1×10^{-6}

800 (CG)	0	2.2×10^{-14}	1.1×10^{-12}	2.2×10^{-11}	7.4×10^{-9}
900 (CG)	0	1.6×10^{-14}	8.4×10^{-12}	7.2×10^{-12}	6.0×10^{-9}
1000 (CG)	0	7.4×10^{-13}	6.4×10^{-11}	3.9×10^{-11}	6.9×10^{-9}
1100 (CG)	0	6.6×10^{-12}	5.3×10^{-10}	5.4×10^{-10}	1.1×10^{-7}
1200 (CG)	0	1.9×10^{-10}	3.5×10^{-9}	5.7×10^{-10}	1.7×10^{-8}
1300 (CG)	0	7.3×10^{-11}	2.2×10^{-9}	3.0×10^{-9}	8.4×10^{-8}
1400 (CG)	0	8.9×10^{-11}	2.3×10^{-9}	4.9×10^{-9}	4.4×10^{-7}
800 (FG)	0	6.7×10^{-15}	3.9×10^{-12}	3.9×10^{-11}	3.2×10^{-8}
900 (FG)	0	6.6×10^{-15}	4.4×10^{-12}	1.0×10^{-11}	1.2×10^{-8}
1000 (FG)	0	4.3×10^{-14}	1.6×10^{-11}	1.9×10^{-11}	5.0×10^{-9}
1100 (FG)	0	4.5×10^{-12}	3.4×10^{-10}	3.9×10^{-10}	3.0×10^{-8}
1200 (FG)	0	2.9×10^{-11}	1.3×10^{-9}	8.5×10^{-10}	4.5×10^{-8}
1300 (FG)	0	5.0×10^{-11}	2.3×10^{-9}	9.7×10^{-10}	8.7×10^{-8}
1400 (FG)	0	3.2×10^{-11}	1.1×10^{-9}	5.0×10^{-9}	2.7×10^{-7}
1000 (FG)	1700	2.9×10^{-14}	1.6×10^{-11}	6.7×10^{-11}	7.5×10^{-8}
1200 (FG)	1700	8.0×10^{-12}	7.5×10^{-10}	4.0×10^{-10}	5.5×10^{-7}
1400 (FG)	1700	4.7×10^{-10}	1.1×10^{-11}	8.7×10^{-9}	5.0×10^{-7}
1000 (FG)	3400	2.6×10^{-15}	2.5×10^{-12}	3.4×10^{-11}	4.6×10^{-8}
1200 (FG)	3400	5.6×10^{-12}	6.0×10^{-10}	2.7×10^{-10}	2.2×10^{-7}
1400 (FG)	3400	3.4×10^{-10}	8.8×10^{-9}	1.2×10^{-8}	7.1×10^{-7}
1000 (FG)	5100	8.9×10^{-15}	8.7×10^{-12}	5.5×10^{-11}	7.3×10^{-8}
1200 (FG)	5100	5.0×10^{-12}	5.6×10^{-10}	4.0×10^{-10}	3.0×10^{-7}
1400 (FG)	5100	2.4×10^{-10}	7.7×10^{-9}	9.1×10^{-9}	5.3×10^{-7}

Table 2: Kinetic constants deduced from the application of parabolic, cubic and paralinear models to mass gain curves under dry air and wet air for single crystal samples (SC), fine-grained (FG) and coarse-grained (CG) polycrystalline samples.

3.2.2. Gas volatilization in dry and wet conditions

In figure 6-A, the gas partial pressure deduced from the volatilization kinetic constant k_v [18] in dry air shows that the paralinear model highlights gas species volatilization above 1200 °C for the Cr_2AlC single-crystals, coarse-grained and fine-grained polycrystalline samples. According to literature [9], this gas should be mostly composed of carbon oxides which is corroborated by the thermodynamic calculations shown in figure 6-B. Indeed, during the dry air oxidation process, the carbon oxides' partial pressure increases supposedly due to the oxidation of the carbides, prevailing on other gas products by far.

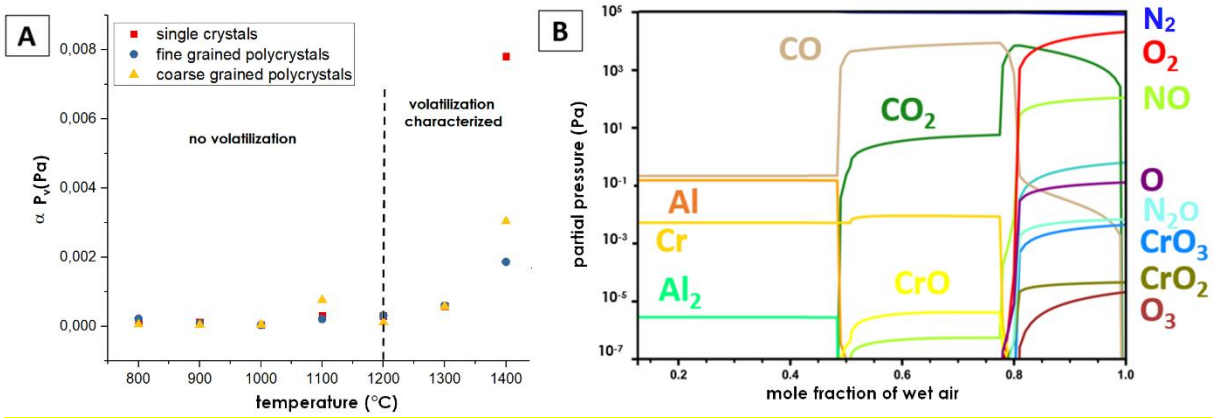

Figure 6: A) Evaporated gas partial pressures deduced from the volatilization kinetic constant of Cr_2AlC single crystal, fine and coarse-grained samples oxidized in dry air during 100 hours in the temperature range 800-1400 °C. The dashed line draws the limit between the temperature (T>1200°C) where gas volatilization occurs or not (T<1200°C). B) CALPHAD calculations of the oxidation product's partial pressures at 1200 °C under dry air.

In Figure 7-A, the gas partial pressure calculated from the volatilization kinetic constant in wet air shows that there is a significantly higher volatilization of species during wet air oxidation than during dry air oxidation for Cr_2AlC fine-grained samples, at least for temperatures higher than 1000°C. Such a result may be associated to oxyhydroxide formation leading to the volatilization of the oxide scale [18]. Nevertheless, alumina is the only oxide formed at this stage and it is not subject to volatilization at such temperatures [19]. Thus, gas volatilization indirectly confirms that the chromium carbide is oxidized. As a consequence, acceleration of volatilization is associated to the acceleration of the chromium carbide oxidation under wet air conditions. By extension, such a result proves the whole Cr_2AlC oxidation process acceleration which is in good agreement with the thick alumina scale observed on the samples oxidized 40h in wet air. It is worth noting that the experimental carbon oxide partial pressure cannot be directly compared to the one predicted by thermodynamic calculations as the gas pressure depends on the kinetic factors.

In Figure 7-B, thermodynamic calculations show that the partial pressures of oxyhydroxide species are much lower than the carbon oxide ones. As a consequence, the gas formation mostly consists in carbon oxides due to the oxidation of the chromium carbide, whose oxidation rate increases in the presence of water vapor. Indeed, the presence of water vapor drastically increases the formed gas pressure as shown in Figure 7-A. Moreover, the gas pressure does not vary significantly with water vapor pressure which likely implies that water vapor is in excess during the chromium carbide oxidation.

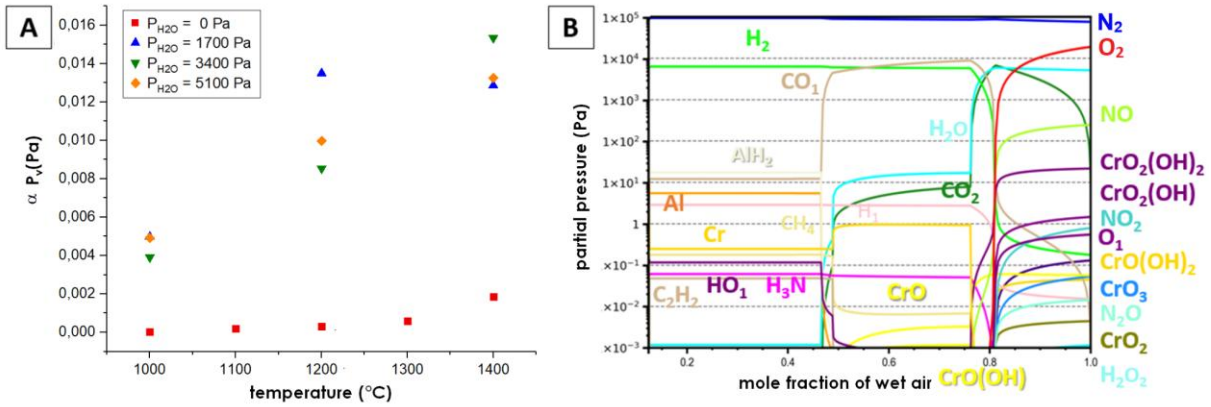

Figure 7: A- Evaporated gas partial pressures deduced from the volatilization constant of Cr_2AlC fine-grained samples oxidized in wet air during 40 hours and in dry air during 100 hours in the temperature range 1000-1400 °C. B- CALPHAD calculations of the oxidation product's partial pressures at 1200 °C under wet air (P_{H_2O}=5100 Pa).

Thermodynamic calculation also predicts the reduction of the water vapor in parallel of the oxidation process, which produce dihydrogen gas, along with other gas state reactions producing NO_X and H_2O_2 gases. These reactions are disregarded since they are supposed to be of minor influence on the total mass variation.

3.2.4. Arrhenius plots

The ln(k_c) are plotted as a function of 1/T to determine the activation energy of the oxidation mechanism. The Arrhenius plots of the cubic model for the oxide growth are reported in Figure 8-A for Cr_2AlC single crystals, fine and coarse-grained samples after 100 hours oxidation in dry air in the temperature range 800-1400 °C. It is the only model to be shown as it is commonly admitted that it is the one that best describes the oxide growth [3]. Moreover, it has been previously mentioned that gas volatilization has only a low influence on the mass gain curve for dry oxidation tests at temperatures below 1200°C.

The Arrhenius curves deduced from the cubic kinetic constants of the dry oxidation tests show a slope variation at low (below 900°C) and high (above 1200°C) temperatures independently of the microstructure. The slope change at 900°C likely results from the oxidation mechanism being, at least partially, driven by surface reactions. The slope change observed at high temperature results from a modification of the oxidation mechanism and is concomitant with the carbon oxide volatilization characterized for T>1200°C in dry air, confirming the oxidation of the chromium carbide sublayer. This chromium carbide oxidation explains the formation of the chromia-rich oxide scale for high enough temperature or oxidation duration in the case of dry air oxidation tests [17].

The Arrhenius plots deduced from the cubic kinetic constants of the wet oxidation tests related to the fine-grained samples are shown in Figure 8-B. The linear shape is typical of a single oxidation mechanism in the investigated temperature range. The deduced activation energies, in the range 430-530 kJ.mol^{-1}, are higher than the activation energy in the linear regime of the dry oxidation tests on fine grained samples between 900 and 1300 °C, reaching a maximum of 400 kJ.mol^{-1}[17]. These values are compatible with the highest values expected in the case of Cr_2AlC oxidation process governed by oxygen diffusion at the grains boundaries [3, 5]. In this case, the oxide growth results from oxygen anions diffusion at the grain boundaries of alumina whereas a weak carbon oxide volatilization also occurs resulting from the Cr_7C_3 carbide oxidation.

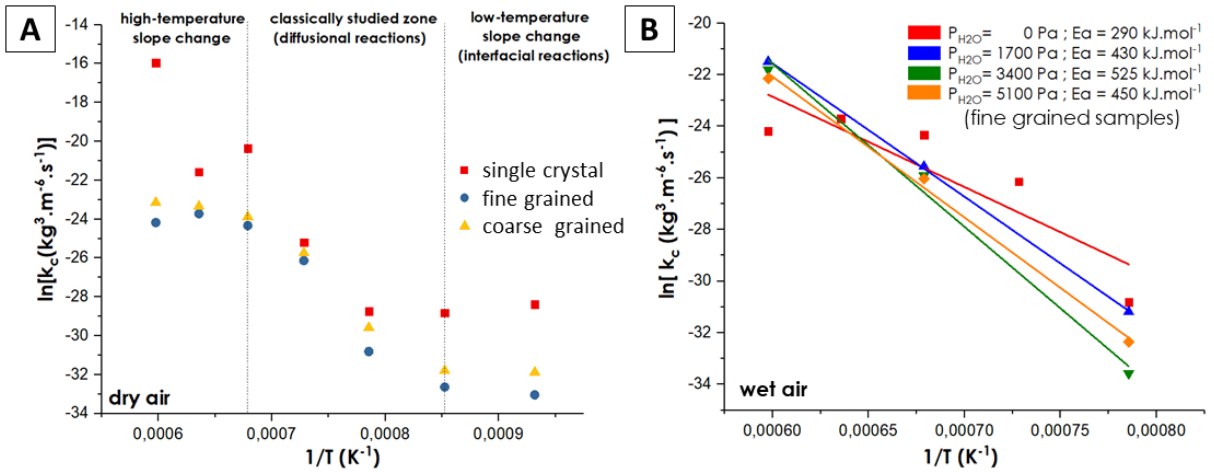

Figure 8: A) Arrhenius plots of cubic kinetic constants of Cr_2AlC single crystals, fine and coarse-grained samples after 100 hours oxidation in dry air in the temperature range 800-1400 °C; B) Arrhenius plots of cubic kinetic constants of Cr_2AlC fine-grained samples after 40 hours oxidation in wet air in the temperature range 1000-1400 °C.

3.2.5. Long duration oxidation tests in wet air

A longer oxidation test (360 hours) at 1400°C with a higher water vapor content (P_{H_2O} = 20 kPa) was carried out on the Cr_2AlC fine-grained sample to observe the gas volatilization. The mass gain curve, shown in Figure 9, can be fitted with an oxide growth part, represented by a cubic law and a volatilization part, represented by a linear law. The resulting kinetic constants (k_c and k_v) match quite well the constants determined in the Table 2 for an oxidation test performed at 1400 °C during 100h under wet air. The small spacing between the experimental and theoretical curves starting at about 20000 s and remaining constant (green arrows) is due to anomalous mass variations associated with external factors (machine related), however one can observe a good match in the evolution of the curves. This experiment is proof of the volatilization phenomena previously determined with mass gain curve's analysis.

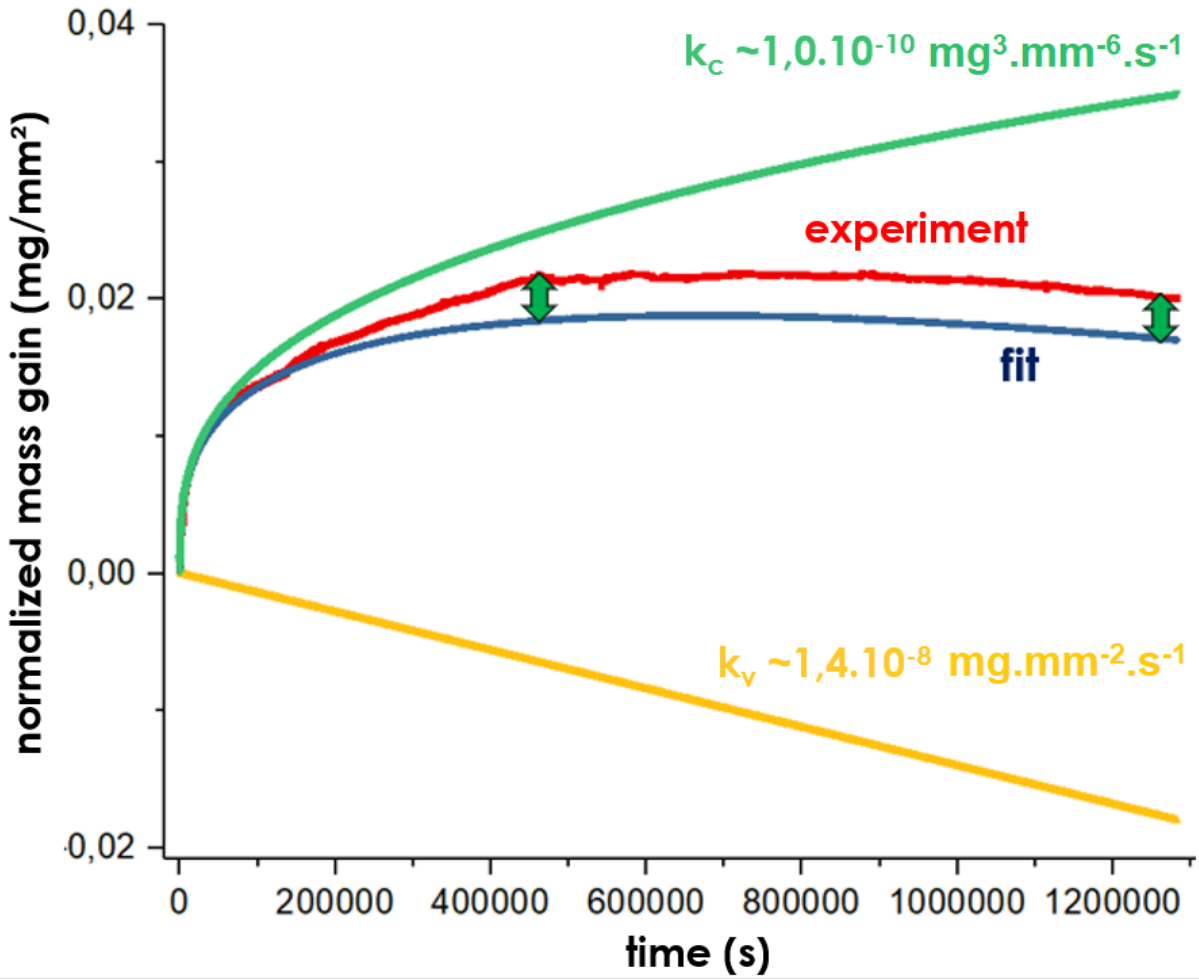

Figure 9: Normalized mass gain curve of a fine-grained Cr_2AlC sample oxidized 360 hours at 1400 °C under wet air (P_{H_2O}= 20 kPa) (red) with a theoretical fit (blue) composed of a cubic law for oxide growth (green) and a linear law for oxide volatilization (yellow).

The higher partial pressure of gaseous species produced during wet air oxidation tests is typical of an acceleration of the oxidation process as observed in numerous studies [19] and confirmed by the long-term oxidation test. This acceleration of the oxidation process is correlated to the presence of the numerous pores in the chromium carbide layer which may result from gas formation. The presence of pores could be also related to the well-known Kirkendall effect which corresponds to the accelerated diffusion of aluminium towards the surface in contact with air.

3.3. Oxidation mechanism of Cr_2AlC

From the experimental data of the present and previous studies [17] coupled with thermodynamic calculations, an oxidation mechanism is proposed and illustrated in Figure 10. As it was previously demonstrated, Cr_2AlC high-temperature oxidation products' nature and arrangement are not sensitive to water vapor pressure - contrary to the reaction's rate which increases in presence of water vapor. The following mechanism can therefore be applied in both dry and wet conditions:

1) The oxygen reacts at the surface with aluminium atoms of the MAX phase to form an alumina scale and the Al-depleted Cr_2AlC in contact with Al_2O_3 transforms into chromium carbide Cr_7C_3.
2) The alumina scale thickens by inward diffusion of oxygen anions through alumina grain boundaries and the outward diffusion of aluminium cations through Cr_7C_3 allows the alumina to be formed close to the Cr_7C_3/MAX phase interface

3) The alumina layer grows until the chromium carbide sublayer thickens enough to make significant the distance between Cr_2AlC/Cr_7C_3 and Cr_7C_3/Al_2O_3 interfaces. At this stage, we assume that oxygen anions diffusion through the alumina scale up to the chromium carbide is faster than the Al cations diffusion from the inner Cr_2AlC up to the Al_2O_3/Cr_7C_3 interface. Thus, oxygen anions diffuse through alumina and reach the chromium carbide layer which is further oxidized, leading to the chromium carbide's volatilization as carbon oxide gaseous species
4) Then the carbon-depleted Cr_7C_3 layer is further oxidized into chromia, along with some alumina due to the remaining aluminium cations from the MAX phase diffusing through the Cr_7C_3. These phenomena lead to an oxide scale composed of chromia and alumina $(Cr,Al)_2O_3$ (see also ref. 17).
5) With respect to the progress of the chromia-alumina oxide formation, oxygen anions can reach Cr_2AlC and lead to the formation of a new alumina layer and chromium carbide sublayer at the interface between Cr_2AlC and the chromia-alumina oxide scale. Al atoms of Cr_2AlC are oxidized in alumina and the outer Cr_2AlC is transformed into chromium carbide Cr_7C_3.

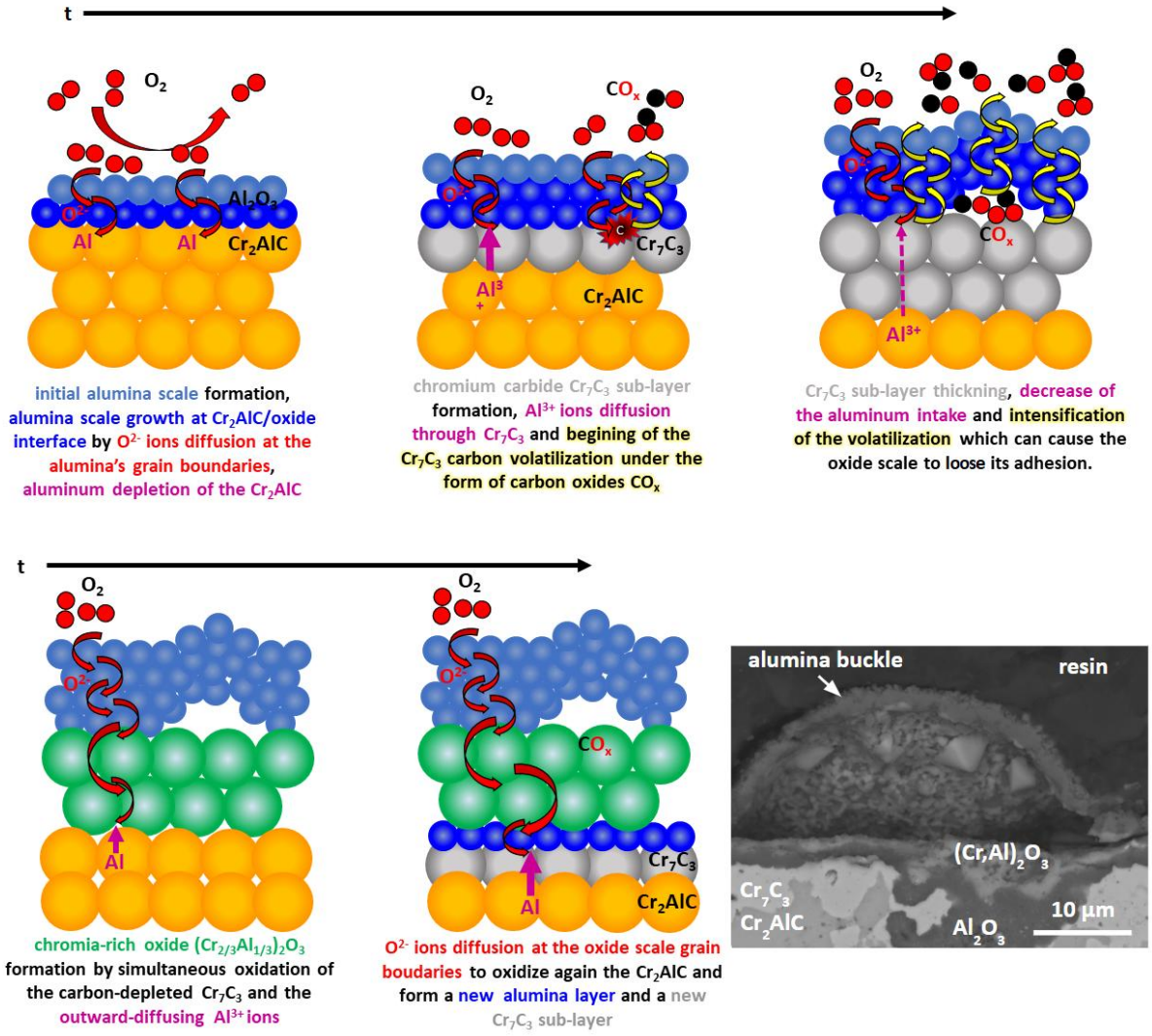

Figure 10: Schematic of the high-temperature oxidation mechanism of Cr_2AlC in air with a final microstructure of a sample oxidized 1000 hours at 1000 °C for comparison.

5. Conclusion

Oxidation tests in dry air were carried out on single crystals, fine and coarse-grained polycrystalline Cr_2AlC samples in the 800-1500 °C range up to 1000 hours [17] whereas oxidation tests in wet air were performed on fine-grained polycrystalline samples in the 1000-1400 °C range up to 360 hours. Thermodynamic calculations were also performed to support experimental investigations. It is demonstrated that oxidation products formed using wet and dry air conditions are similar. They consist in a continuous Al_2O_3 alumina layer, a porous Cr_7C_3 sublayer, as well as progressive gaseous carbon oxide emission due to Cr_7C_3 oxidation, in good agreement with thermodynamic calculations. The water vapor partial pressure does not affect the nature and the arrangement of the oxidation products in the studied range, but it does modify its kinetics by increasing the oxidation rate. Such an increase, during wet air tests, is correlated to the higher partial pressure of carbon oxides produced in the presence of humidity. Lastly, based on thermodynamic calculations, kinetics and microstructural analyses related to wet and dry air oxidation tests, a complete oxidation mechanism has been proposed for pure Cr_2AlC.

6. Acknowledgement

Special thanks to the Région Nouvelle-Aquitaine and the Ministère de l'Enseignement Supérieur et de la Recherche for funding this research. This work was supported by the French government program “Investissements d’Avenir” (EUR INTREE, reference ANR-18-EURE-0010). This work was supported by the European commission through the Horizon 2020 project IL TROVATORE (n° 740415).

7. References

[1] M. Sokol, V. Natu, S. Kota, M. W. Barsoum. On the Chemical Diversity of the MAX Phases. Trends in Chemistry, vol. 1, n°2, p.210-223, 2019. https://doi.org/10.1016/j.trechm.2019.02.016

[2] J. Jeitschko, H. Nowotny, F. Benesovsky. Kohlenstoffhaltige ternäre Verbindungen (H-Phase). Monatshefte für Chemie, vol. 94, n°4, p.672-676, 1963. https://doi.org/10.1007/BF00913068

[3] D. J. Tallman, B. Anasori, M. W. Barsoum. A Critical Review of the Oxidation of Ti_2AlC, Ti_3AlC_2 and Cr_2AlC in air. Materials Research Letters, vol. 1, n°3, p.115-125, 2013. https://doi.org/10.1080/21663831.2013.806364

[4] Z. Lin, M. Zhuo, Y. Zhou, M. Wang. Atomic scale characterization of layered ternary Cr_2AlC ceramic. Journal of Applied Physics, vol. 99, n°7, p.076109, 2006. https://doi.org/10.1063/1.2188074

[5] J. L. Smialek. Oxygen diffusivity in alumina scales grown on Al-MAX phases. Corrosion Science, vol. 91, p.281-286, 2015. https://doi.org/10.1016/j.corsci.2014.11.030

[6] C. D. Tossey, B. M. Tossey. High temperature oxidation of corrosion resistant alloys from machine learning. npj Materials Degradation, vol. 5, n°1, p.1-10, 2021. https://doi.org/10.1038/s41529-021-00184-3

[7] Ashby, M.F. The CES EduPack Resource Booklet 2: Material and Process Selection Charts. 2009. http://www.grantadesign.com/download/pdf/teaching_resource_books/2-Materials-Charts-2010.pdf

[8] D.B. Lee, T.D. Nguyen, J.H. Han, S.W. Park. Oxidation of Cr_2AlC at 1300 °C in air. Corrosion Science, vol. 49, pp. 3926–3934, 2007. https://doi.org/10.1080/21663831.2013.806364

[9] Z.J. Lin, M.S. Li, J.Y. Wang, Y.C. Zhou. High-temperature oxidation and hot corrosion of Cr_2AlC. Acta Materialia, vol. 55, pp. 6182–6191, 2007. https://doi.org/10.1016/j.actamat.2007.07.024

[10] D.B. Lee, S.W. Park. Oxidation of Cr_2AlC between 900 and 1200 °C in air. Oxidation of Metals, vol. 68, pp. 211–222, 2007. https://doi.org/10.1007/s11085-007-9071-0

[11] W. Tian, P. Wang, Y. Kan, G. Zhang. Oxidation behavior of Cr_2AlC ceramics at 1,100 and 1,250 °C. Journal of Materials Science, vol. 43, pp. 2785–2791, 2008. https://doi.org/10.1007/s10853-008-2516-2

[12] D.B. Lee, T.D. Nguyen. Cyclic oxidation of Cr_2AlC between 1000 and 1300 °C in air. Journal of Alloys and Compounds, vol. 464, pp. 434–439, 2008. https://doi.org/10.1016/j.jallcom.2007.10.018

[13] D.B. Lee, T.D Nguyen, S.W. Park. Long-time oxidation of Cr_2AlC between 700 and 1,000 °C in air. Oxidation of Metals, vol. 77, pp. 275–287, 2012. https://doi.org/10.1007/s11085-012-9285-7

[14] S. Li, L. Xia, G. Song, X. Wu, W.G. Sloof, S. van der Zwaag. Oxidation and crack healing behavior of a fine-grained Cr_2AlC ceramic. Journal of the American Ceramic Society, vol. 96, pp. 892–899, 2013. https://doi.org/10.1111/jace.12170

[15] S. Li, X. Chen, Y. Zhou, G. Song. Influence of grain size on high temperature oxidation behavior of Cr_2AlC ceramics. Ceramics International, vol. 39, pp. 2715–2721, 2013. https://doi.org/10.1016/j.ceramint.2012.09.039

[16] J. Gonzalez-Julian, T. Go, D.E. Mack, R. Vaßen. Environmental resistance of Cr2AlC MAX phase under thermal gradient loading using a burner rig. Journal of American Ceramic Society, vol. 101, pp. 1841-1846, 2018. https://doi.org/10.1111/jace.15425

[17] A. Zuber, V. Gauthier-Brunet, J. Roger, J. Gonzalez-Julian, T. Ouisse, S. Dubois. Towards a better understanding of the high-temperature oxidation of MAX phase Cr_2AlC. *Journal of the European Ceramic Society*, vol. 42, p.2089-2096, 2022. https://doi.org/10.1016/j.jeurceramsoc.2021.12.057

[18] E. J. Opila, D. L. Myers. Alumina volatility in water vapor at elevated temperatures : application to combustion environments. NTRS-NASA Technical Reports Server, ID n°20030111832, 2003. https://ntrs.nasa.gov/citations/20030111832

[19] E. J. Opila. Volatility of Common Protective Oxides in High-Temperature Water Vapor: Current Understanding and Unanswered Questions. Materials Science Forum, vol. 461-464, p.757-774, 2004.

https://doi.org/10.4028/www.scientific.net/MSF.461-464.765

[20] D. L. Douglass, P. Kofstad, P. Rahmel, G. C. Wood. International Workshop on High-Temperature Corrosion. Oxidation of Metals, vol. 45, issue 5-6, pp. 529-620, 1996. https://doi.org/10.1007/BF01046850

[21] S. R. J. Saunders, M. Monteiro, F. Rizzo. The oxidation behaviour of metals and alloys at high temperatures in atmospheres containing water vapour: A review. Progress in Materials Science, vol. 53, pp.755-837, 2008. https://doi.org/10.1016/j.pmatsci.2007.11.001

[22] Z. J. Lin, M. S. Li, J. Y. Wang, Y. C. Zhou. Influence of water vapor on the oxidation behavior of Ti_3AlC_2 and Ti_2AlC. Scripta Materialia, vol. 58, pp. 29-32, 2008. https://doi.org/10.1016/j.scriptamat.2007.09.011

[23] P. Berthod. Kinetics of High Temperature Oxidation and Chromia Volatilization for a Binary Ni–Cr Alloy. Oxidation of Metals, vol. 64, issue 3-4, p.235-252, 2005. https://doi.org/10.1007/s11085-005-6562-8

[24] J.-O. Andersson, T. Helander, L. Höglund, P. Shi, B. Sundman. Thermo-calc and dictra. CALPHAD, vol. 26, pp. 273–312, 2002. https://doi.org/10.1016/S0364-5916(02)00037-8

[25] B.Sundman, H.L. Lukas, S.G. Fries. Computational thermodynamics: the calphad method. Cambridge University Press, 2007.

[26] B. Hallstedt, D. Music, Z. Sun. Thermodynamic evaluation of the Al-Cr-C system. Zeitschrift für Metallkunde, vol. 97, pp. 539-542, 2006. https://doi.org/10.3139/146.101270

[27] T.M. Besmann, N.S. Kulkarni, K.E. Spear. Thermochemical analysis and modelling of the Al_2O_3 - Cr_2O_3, Cr_2O_3 -SiO_2, and Al_2O_3 -Cr_2O_3 -SiO_2 systems relevant to refractories. Journal of American Ceramic Society, vol. 89, pp. 638–644, 2006. https://doi.org/10.1111/j.1551-2916.2005.00719.x

[28] P. J. Linstrom, W.G. Mallard. NIST chemistry webbook, NIST standard reference database 69 [data set]. National Institute of Standards and Technology. 1997.

[29] B.B. Ebbinghaus. Thermodynamics of gas phase chromium species: The chromium oxides, the chromium oxyhydroxides, and volatility calculations in waste incineration processes. Combustion and flame, vol. 93, pp. 119–137, 1993. https://doi.org/10.1016/0010-2180(93)90087-J

[30] A. Jain, S.P. Ong, G. Hautier, W. Chen, W.D. Richards, S. Dacek, S. Cholia, D. Gunter, D. Skinner, G. Ceder, K.A. Persson. The Materials Project: A materials genome approach to accelerating materials innovation. APL Materials, vol. 1, issue 1, p. 011002, 2013. https://doi.org/10.1063/1.4812323